Solar Energy Materials & Solar Cells 293 (2025) 113830

Contents lists available at ScienceDirect

Solar Energy Materials and Solar Cells

journal homepage: www.elsevier.com/locate/solmat

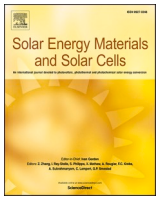

How the selenium is affecting the physical and electrical properties of ultra-thin CdSeTe/CdTe solar cells

Mariyam Mukhtar [d], Elisa Artegiani [d], Sam Machin [a], Andrea Gasparotto [b], Chiara Liliana Boldrini [c], Giorgio Tseberlidis [c], Simona Binetti [c], Michael Walls [a], Alessandro Romeo [d,*]

[a] Centre for Renewable Energy Systems Technology (CREST), Wolfson School of Mechanical, Electrical and Manufacturing Engineering, Loughborough University, Leicestershire, LE11 3TU, UK
[b] Department of Physics and Astronomy "G. Galilei", University of Padova, Padova, Italy
[c] Department of Materials Science and MIBSOLAR Center, University of Milano-Bicocca, Milan, Italy
[d] Laboratory for Photovoltaics and Solid-State Physics (LAPS), Department of Computer Science, University of Verona, Strada le Grazie 15, Verona, 37134, Italy

ARTICLE INFO

Keywords:
CdSeTe/CdTe
Ultra-thin absorber
Solar cells
Thin film

ABSTRACT

The incorporation of selenium into the CdTe has recently enhanced the performance of the solar cells to 23.1 %. The narrower band gap of the CdSeTe/CdTe absorber boosts the short-circuit current density; also, Se introduction increases the carrier's lifetime. Optimizing $CdSe_xTe_{1-x}$ band-grading is crucial for achieving high-performance CdTe photovoltaics. Another current goal is to reduce the thickness of the absorber to further reduce production costs and environmental impact. Thus, studying the effects of Se introduction in ultra-thin CdTe absorbers is essential. To investigate Se concentration's impact on ultra-thin CdTe, we fabricated CdSeTe/CdTe devices with an absorber thickness of 0.8 μm by depositing different CdSe/CdTe ratios. Our 0.8 μm thick cells have currently achieved an efficiency of 12.8 %, but most important this study shows that Se introduction in ultra-thin CdTe results in structural properties different from those of thicker absorbers, impacting the device performance.

1. Introduction

Over the past twenty years, several key improvements have resulted in advancements in CdTe photovoltaic (PV) efficiency, which has reached 23.1 % [1]. One significant enhancement is related to selenium introduction to form a graded $CdSe_xTe_{1-x}$/CdTe absorber. The presence of $CdSe_xTe_{1-x}$ near the junction reduces the band gap to around 1.4 eV, broadening the wavelength range for photocurrent generation [2]. This approach, coupled with eliminating the CdS window layer and its parasitic absorption, significantly increases the short-circuit current density (Jsc), which now exceeds 30 mA cm^{-2} [3].

Additionally, selenium introduction improves the carrier lifetime by reducing nonradiative recombination into the absorber, resulting in an open-circuit voltage comparable to that of CdTe despite its narrower band gap [4].

Another important aspect, nowadays, is the reduction of the absorber thickness to save material and further reduce production costs [5–7]. Theoretically, CdTe high optical absorption coefficient would allow incoming light with energy over its band gap to be completely absorbed within 1 μm from the surface [8]. However, the reduction in thickness is not a linear process because it influences the physical and electrical properties of the absorber. Problems such as hole formation, reduced crystallization, and possible material diffusion within the interfaces may also be encountered [9].

Moreover, despite CdTe being a stable compound and not releasing Cd (it is not on the list of carcinogenic materials) [10], it is subjected to RoHS (Restriction of Hazardous Substances) directives in the European Union. RoHS regulates the maximum concentration in consumer electronic items of elements considered dangerous to humans, and cadmium is limited to 0.01 % or 100 ppm by weight. This means that using an absorber thickness below 0.8 μm would make CdTe-based devices on a 3 mm thick glass RoHS compliant, further expanding the possible applications of this technology [11].

So studying the impact of selenium and its concentration in an ultra-

* Corresponding author.
E-mail address: alessandro.romeo@univr.it (A. Romeo).

https://doi.org/10.1016/j.solmat.2025.113830
Received 15 April 2025; Received in revised form 2 July 2025; Accepted 4 July 2025
Available online 12 July 2025

thin absorber layer becomes a very important issue. In order to understand the mechanisms of Se impact on ultra-thin devices, we have reduced the thickness of our absorber to 800 nm, and we have fabricated and analyzed devices with different CdSe/CdTe ratios.

2. Device fabrication

In our laboratory, we fabricate CdTe solar cells in superstrate configuration using a low substrate temperature process [12]. On a commercial glass substrate coated with FTO/TO (SnO_2: F/SnO_2), named TEC 12D, we deposit a CdSe layer followed by a CdTe layer by vacuum evaporation, keeping the temperature of the substrate at 340 °C. During the deposition, the film thickness is measured using a quartz crystal microbalance placed next to the substrate holder and cross-checked with a stylus profilometer. For this specific study, we have reduced the thickness of the absorber from our standard 2 μm [13] to 0.8 μm. Precisely, we have fabricated different devices depositing CdSe/CdTe with various ratios: 75/725 nm, 150/650 nm, 270/530 nm, and 400/400 nm.

Later, the activation treatment is applied by drop-casting a $CdCl_2$-methanol solution on the surface and subsequently annealing in air at 390 °C. The $CdCl_2$ treatment also mixes the CdSe/CdTe layers to generate the expected $CdSe_xTe_{1-x}$ compound towards the junction [14]. Finally, the samples are etched in a Br-MeOH solution, which removes the $CdCl_2$ residuals from the surface, simultaneously forming a Te-rich surface that promotes the synthesis of Cu_xTe at the CdTe/back contact junction to improve cell stability [15]. Vacuum evaporation is used to deposit a 0.5 nm thick copper and a 30 nm thick gold layer to form the back contact (Fig. 1). Finally, the sample undergoes an air annealing at 200 °C to diffuse Cu into the absorber. The area of each dot cell is 0.13 cm^2.

3. Characterization methods

The current density-voltage (JV) characteristics were determined using a Keithley Source Meter 2420 under an AM 1.5 spectrum at 100 mW/cm^2 and a LOT Quantum Design Europe solar simulator LS0306.

External Quantum Efficiency (EQE) measurements were recorded using a monochromator (Lot-Oriel Omni-λ300) and a halogen lamp (100 W) as the incident light in AC mode. The monochromatic light was mechanically chopped at a frequency of 75 Hz, and the photocurrent response was measured using a lock-in amplifier. The system was calibrated with Thorlabs S120VC and S122C photodiodes.

An HP4284A LCR performs capacitance-voltage (CV) and drive-level capacitance profiling (DLCP). The measurements were carried out at bias frequencies of 10 kHz at 300K, using a perturbation AC voltage of 50 mV.

The thickness of the film is cross-checked with a customized A.P.E. Research stylus profilometer.

XRD measurements were collected on a Rigaku Miniflex 600 in Bragg-Brentano geometry, with a Cu-Kα source (λ = 1.5446 Å) and a silicon array as the detector.

Secondary Ion Mass Spectrometry (SIMS) depth profiles were achieved on a CAMECA IMS-4f using a Cs + primary ion beam at a 10 kV accelerating voltage (corresponding to 5.5 keV impact energy) and detection of positive secondary ions.

Electron backscatter diffraction (EBSD) analysis was performed with a Helios G4 (ThermoFisher Inc) equipped with a Xenon-Plasma Focused Ion Beam (pFIB) and a CMOS detector, using an electron beam accelerating voltage of 5 kV and a current of 6.4 nA.

Cathodoluminescence (CL) measurements were performed at room temperature in a thermal field emission SEM equipped with a Monarc Pro CL system, with an electron beam accelerating voltage of 5 kV and a beam current of 1.6 nA. The CL maps were acquired using a 200 μs dwell time per pixel.

4. Results and discussion

4.1. Structural and electrical analysis

X-ray diffraction (XRD) analysis has been conducted to investigate the crystallographic structure of the absorber and understand how the incorporation of selenium affects its composition. Fig. 2(A) shows the XRD patterns of treated absorbers fabricated with different CdSe/CdTe ratios. Key peaks are identified: the dominant orientation of the CdTe is (111), with smaller peaks at (220), (311), (400) and (331). Moreover, smaller peaks attributed to CdSe are detected, suggesting the presence of remains of this compound. On the right, Fig. 2(B) displays a close-up of the dominant CdTe peaks, highlighting that as the CdSe thickness increases, these peaks shift to the right. This indicates an increasing incorporation of selenium into the crystal lattice, forming a $CdSe_xTe_{1-x}$ compound [16].

Furthermore, the peaks become broader by increasing the thickness of the CdSe layer. According to the kinematic scattering theory, the broadening of the peaks can be attributed to increased lattice defects or a reduction in the crystallite size to less than one micron [17]. For thicker CdSeTe/CdTe absorbers, it has already been experimentally observed that the introduction of selenium into the absorber leads to the formation of a CdSeTe layer with smaller grains towards the junction and a second layer of larger grains from the bulk to the back contact (the absorber tends to form a bi-layer: CdSeTe at the front and CdTe at the

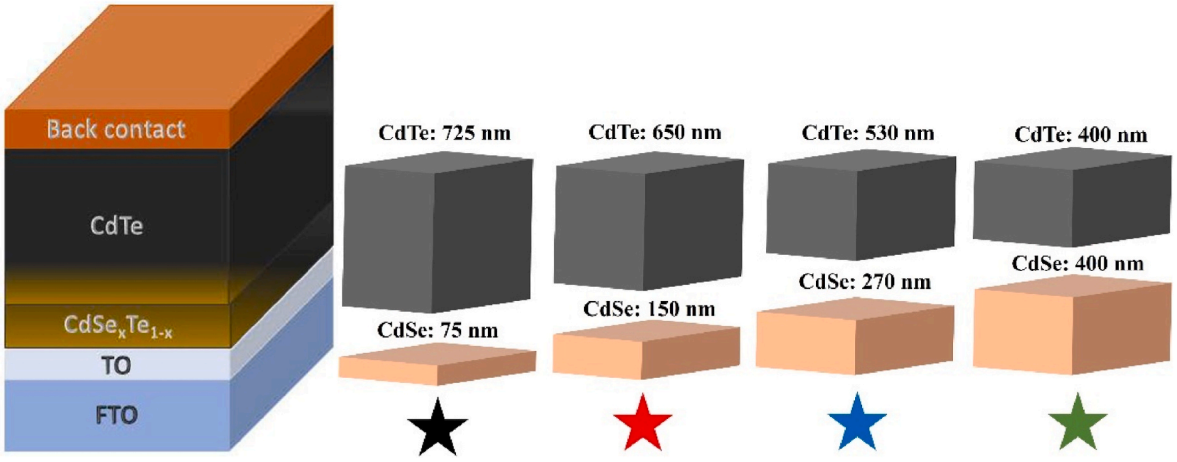

Fig. 1. Sketch of the configuration of the devices fabricated and analyzed (the colored star indicates the colors that will be used in the following graphs for identifying the different cases). (For interpretation of the references to color in this figure legend, the reader is referred to the Web version of this article.)

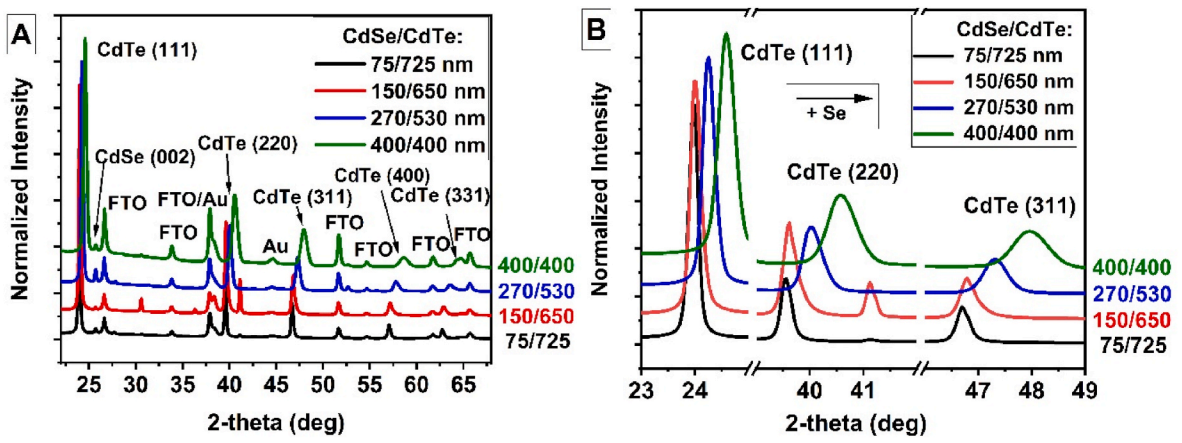

Fig. 2. XRD analysis of samples fabricated with different CdSe/CdTe ratios: (A) 22–68 deg range spectra; (B) close-up of the main CdTe peaks.

back) [18,19]. This effect could also be expected for ultrathin absorbers; the broadening of the peaks could then suggest a preponderance of small grains as the CdSe thickness increases, due to a higher Se incorporation in the CdSeTe compound. Especially in the case of 150/650, we can observe some minor peaks around 2-theta at 31, 41 and 52°, these can be easily attributable to the formation of $CdTeO_x$, occurring with $CdCl_2$ activation treatment [20].

Fig. 3 presents AFM images of $CdSe_xTe_{1-x}$/CdTe films formed by activating a 75/725 nm (Fig. 3(A)) and a 400/400 nm (Fig. 3(B)) CdSe/CdTe bi-layer. The morphology of the absorber turns out to be different. The grains of the 400/400 nm CdSe/CdTe sample are visibly smaller compared to the 75/725 nm, which has much more compact grains. This confirms the hypothesis that the broadening of the XRD peaks is due to a reduction of the absorber layer's grain size by increasing the CdSe layer thickness.

SIMS analysis has been carried out on the samples to address the selenium distribution into the absorbers after the $CdCl_2$ treatment. With a 75 and 150 nm thick CdSe layer, the Se profiles decrease towards the back contact, suggesting a graded band gap absorber (see Fig. 4). Conversely, the corresponding Te profiles are nearly flat. Still, it must be considered that the yield of SIMS measurements depends on the element. As expected, in the 400/400 nm case, the measurement shows a higher amount of Se than the other samples and detects a lower amount of Te. In this case, the Se profile is almost flat, showing only a

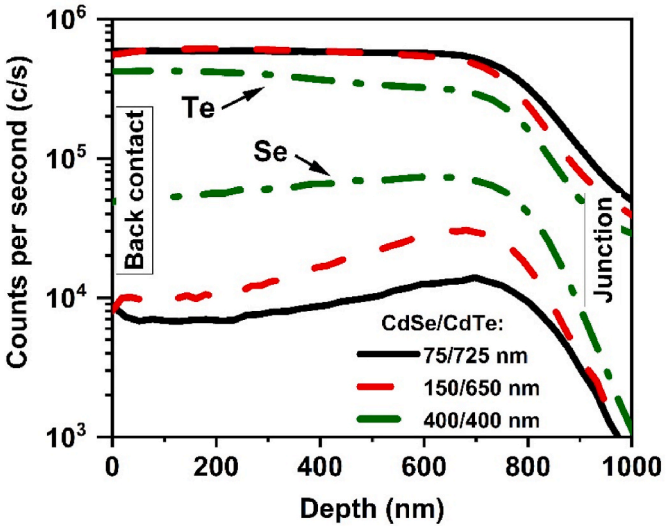

Fig. 4. SIMS depth profiles showing Se and Te distribution in absorbers fabricated with different CdSe/CdTe ratios.

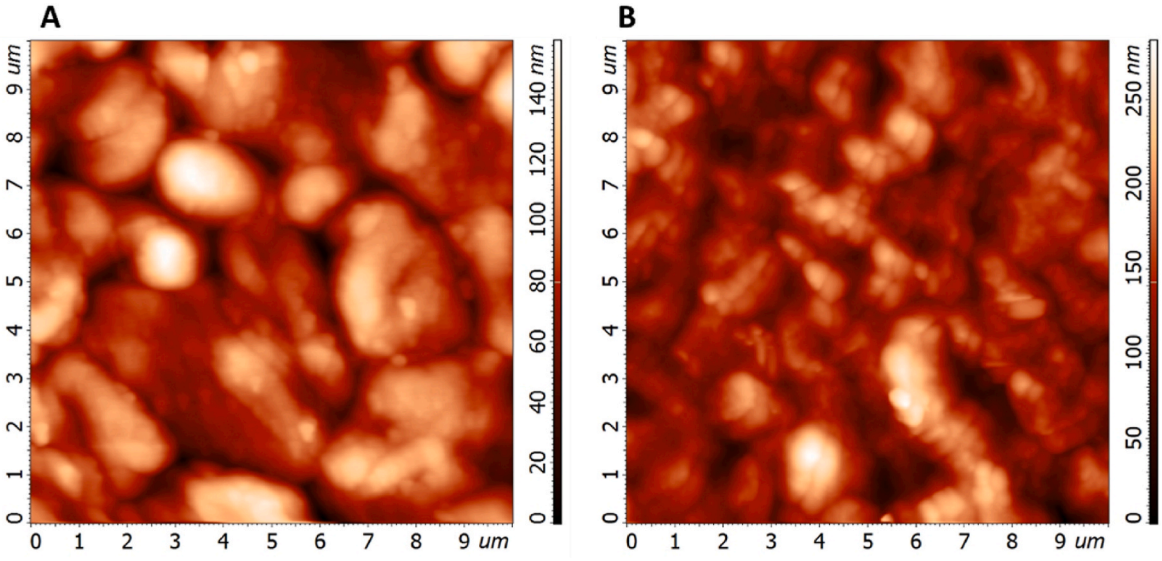

Fig. 3. AFM images of absorber surface of (A) 75/725 nm (B) and 400/400 nm CdSe/CdTe samples.

slight decrease in counts per second towards the back contact, suggesting the formation of a nearly homogeneous CdSeTe composition along the entire depth of the absorber layer. However, in all the devices, Se diffuses throughout the layer. Comparing the devices at corresponding sputtering depths, as the initial CdSe thickness increases, the samples show a more selenium-rich compound throughout the absorber. As already mentioned in the previous paragraph, the presence of Se leads to smaller grains than those of CdTe. Thus, the increasing presence of selenium in the bulk and towards the back contact explains the smaller grains on the back surface of the absorber observed with AFM and the broadening of the XRD peaks in the samples fabricated with thicker CdSe layers.

The samples were subjected to EQE analysis (see Fig. 5) to verify whether selenium, besides being distributed throughout the absorber, reduces the band gap near the junction compared to pure CdTe, increasing the absorption at long wavelengths. Despite the small CdSe peaks detected by XRD, the EQE spectra do not reveal a parasitic absorption below 700 nm for the residual CdSe layer [21], suggesting a quasi-complete intermixing of CdSe and CdTe in all the samples. This appears to be an advantage of using a thin absorber since it was shown that parasitic absorption due to incomplete mixing occurs if 200–400 nm of CdSe is evaporated for a total absorber thickness of 3.5 μm [22].

As the thickness of the CdSe layer in the devices is increased from 75 to 270 nm, the spectra show a right shift of the response at long wavelengths, confirming the narrowing of the band gap of the absorber. Taking the value corresponding to the maximum negative derivative of the EQE curve at long wavelengths [23], the band gaps are estimated to be 1.44 eV with a 75 nm thick CdSe and 1.39 eV with a 270 and 400 nm thick CdSe. A 270 nm thick CdSe on a total absorber thickness of 800 nm is sufficient to reach the minimum band gap achievable with a $CdSe_xTe_{1-x}$ compound. Moreover, the 400/400 sample denotes a noticeable decrease in EQE response at all wavelengths; this loss is not localized but appears uniform throughout the absorber. Such a reduction in EQE generally suggests a higher concentration of defects causing recombination in the entire absorber. In this specific case, one could hypothesize that a more selenium-rich CdSeTe could be associated with a reduced photoactivity; on the other hand, another probably more suitable explanation is that the reduction of the grain size due to the increasing of Se concentration in the bulk (as highlighted by the measurements discussed previously) implies a higher amount of grain boundaries and so a significant carrier recombination.

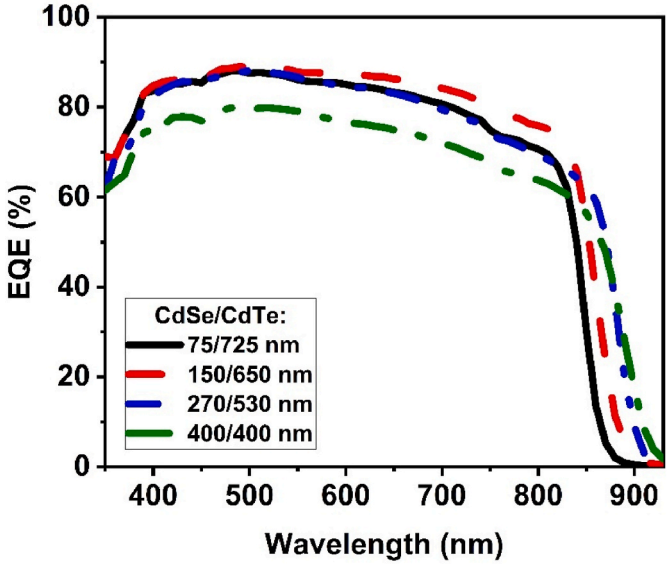

Fig. 5. Comparison of EQE of samples fabricated with different CdSe/CdTe ratios.

To investigate whether this decrease in EQE response is related to the grain size in the absorber and, hence, the amount of grain boundaries, EBSD analysis was performed on the cross-section of 400/400 nm and 75/725 nm samples. EBSD images provide a microstructural analysis, where the colored regions represent the crystallographic orientations of individual grains. For the device with lower selenium concentration (see Fig. 6(A)), the grains are approximately equiaxed, with an average size of 1.1 μm throughout the absorber layer. Moreover, most grains occupy the entire thickness of the absorber, from the front to the back surface. On the other hand, the 400/400 nm sample exhibits a smaller grain size of 0.86 μm on average (see Fig. 6(B)). A few grains extend from the front to the back surface, but mostly, the structure is disordered with smaller overlapping grains; dark areas highlight the presence of voids. Interestingly, no sample shows evidence of a CdSeTe/CdTe bilayer structure, as observed for thicker absorbers [18]. This analysis confirms that with the increase of the CdSe thickness, the grain size reduces in the whole absorber, not only near the junction; and this is because by using a 0.8 μm thick absorber, there is no formation of a CdSeTe/CdTe bi-layer structure. Moreover, it suggests that a high selenium concentration leads to a disordered arrangement of the grains, and also to the formation of voids (confirmed by cross-sectional backscatter SEM images, not shown here), contributing to the reduced EQE response seen before.

SIMS analysis indicates a different Se diffusion and EQE analysis points out the presence of a different band gap in the 75/725 and 150/650 nm absorbers; however, the absence of a CdSeTe/CdTe bi-layer structure highlighted by EBSD images is unusual. To investigate this phenomenon in detail, SEM was used to collect the CL hyperspectral map of the 75/725 and 400/400 nm samples compared to the standard thick absorber sample in cross-section (see Fig. 7); colour variations correspond to emission energy (eV) differences, showing localized variations in the band gap. Fig. 7(B) confirms the formation of a nearly homogeneous CdSeTe composition of the absorber layer for the 400/400 nm case, as assumed by SIMS profiles. The dark blue region in the absorber in Fig. 7(B) corresponds to a uniform bandgap energy of 1.39 eV. Note that the scattered red and white pixels surrounding this region of the absorber are due to detector noise. On the other hand, for the 75/725 nm case (Fig. 7(A)), the CL signal shows a band gap ranging from 1.43 eV to 1.47 eV. However, the map suggests that the band gap is not graded from the front junction to the back, perpendicularly to the substrate, but varies from grain to grain. Selenium is supposed to diffuse along the grain boundaries and subsequently into the CdTe grains through the grain boundaries [24]. Fig. 7c is there to show that with a standard thickness, the absorber shows its expected grading, highlighting that the behavior described above is to be addressed to the ultra-thin absorber.

However, the question of whether, during recrystallization, Se preferentially diffuses in some grains rather than others has never been addressed. One hypothesis is that this might depend on the initial orientation of the grains: from the grain boundaries, the selenium enters the near grains with an orientation more favourable to its diffusion. With a CdTe thickness less than 800 nm, the size of the grains extends from front to back contact even for as-deposited samples, i.e. before the activation treatment; selenium, therefore, appears to be unable to penetrate some grains whose orientation is possibly unfavorable to its diffusion. In the case of a 2–3 μm thick CdTe, the thickness of the as-deposited absorber is composed of a few layers of grains; selenium diffusing across grain boundaries can then surround the grains of the first layer/layers, finding the most energetically favourable path to diffuse inside as well. This also explains why, using larger thicknesses, a CdSeTe/CdTe bi-layer is formed. The diffusion of Se in the first layers of grains forms the CdSeTe layer, while Se does not affect the subsequent grain layers, which, therefore, remain CdTe. This bi-layer cannot form if the grains of the as-deposited CdTe extend throughout the entire thickness of the film.

The integration of EBSD, CL and EBSD GB misorientation measurement (Aztec) can identify if this supposition is correct. In Fig. 8, the

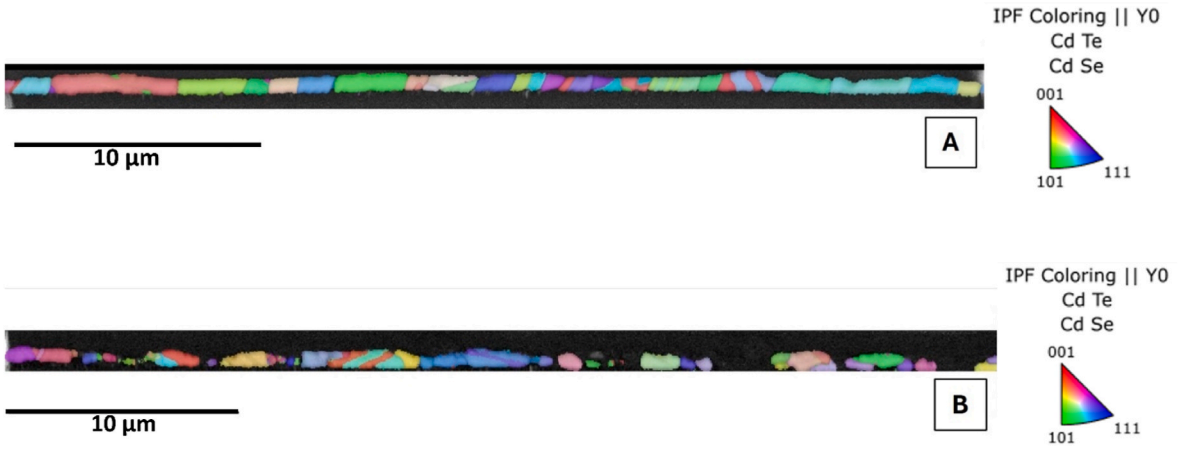

Fig. 6. EBSD analysis of samples (A) 75/725 nm and (B) 400/400 nm in cross-section.

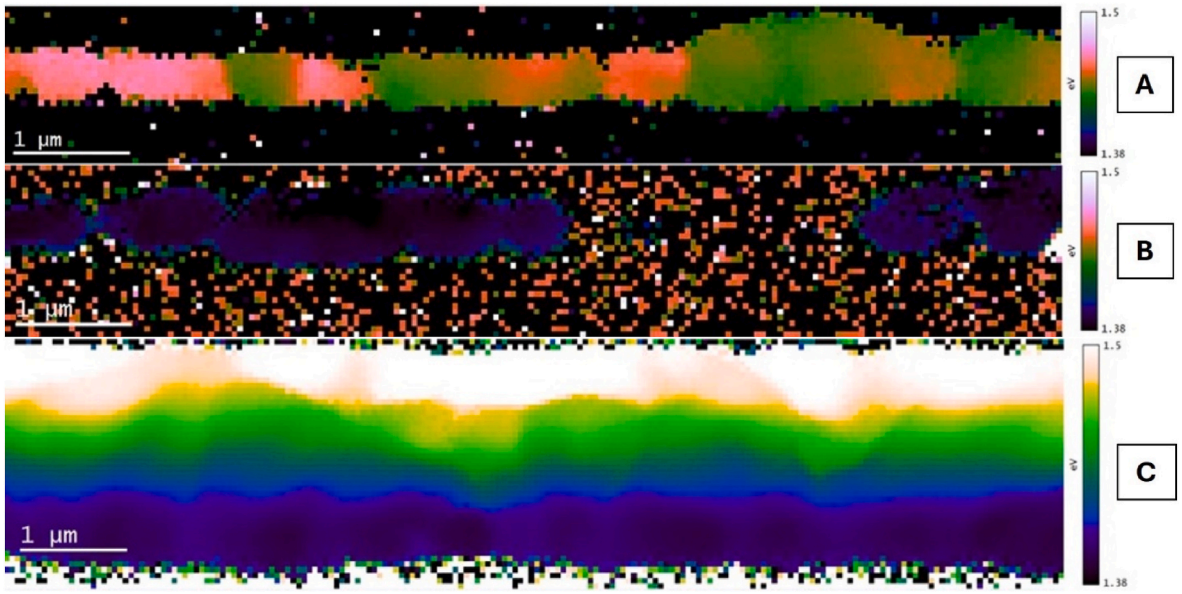

Fig. 7. Hyperspectral CL map (eV) of the (A) 75/725 nm, (B) 400/400 nm, and (C) 300/2000 nm devices.

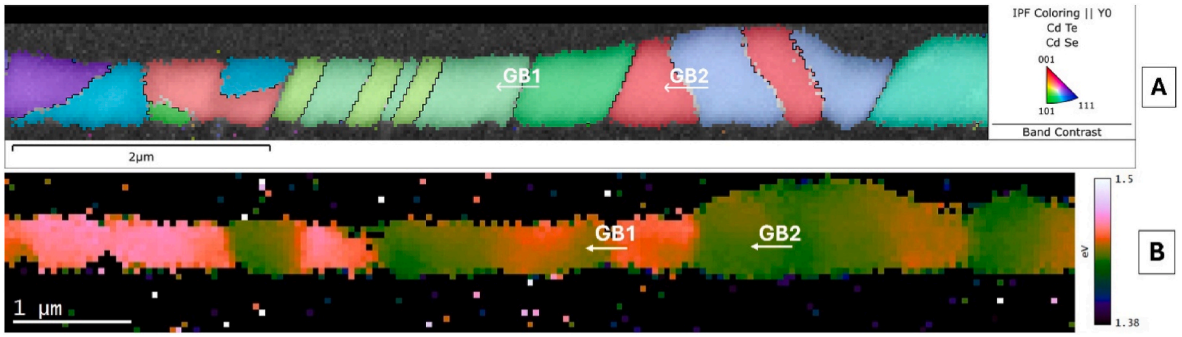

Fig. 8. (A) EBSD map and (B) cathodoluminescence (CL) map of the same region of the CdTe absorber, showing two grain boundaries labelled GB1 and GB2. These boundaries are marked to enable direct comparison between crystallographic features and CL response. The misorientation angles are 15.14° for GB1 and 59.93° for GB2, respectively.

specific area of the 75/725 nm case, depicted in Fig. 7(A), is analyzed by Aztec: grain boundary (GB) misorientation angles can be determined for any grain. In this case we have isolated two boundaries; the LHS boundary (GB1) has a misorientation angle of 15.14°, a low angled boundary whose neighbouring grain interior's colouring in the hyperspectral CL map indicates that the GB acts as a barrier between a relatively high Se content grain to its left, and low Se content to its right. The RHS GB misorientation angle of 59.93° (GB2) is much higher and is

classified as a Σ3 boundary. The higher grain boundary misorientation angle has allowed more lateral Se diffusion, leading to lower band gap readings at neighbouring grain interiors, as shown in the CL hyperspectral map. Essentially, higher grain boundary misorientation angles encourage more Se diffusion between grains, whereas lower grain boundary misorientation angles inhibit Se diffusion.

To further investigate the impact of selenium concentration on the presence of defects, CV and DLCP analyses were performed on the samples (see Fig. 9). CV and DLCP measurements enable the estimation of the net charge density (difference between acceptor and donor states) as a function of distance from the junction. Since deep defects have minimal impact on the DLCP profiles (solid dots), the discrepancy between the CV (open dots) and DLCP curves, recorded under identical frequency and temperature conditions, reveals the amount of deep defects [25]. Furthermore, the arrows correspond to the point of the measurement taken when the DC bias voltage is equal to 0, estimating the width of the depletion region. As the CdSe thickness increases, CV profiles go from being lower to being higher than DLCP profiles, suggesting a different nature of the deep defects. For lower selenium concentrations, the deep defects compensate the net charge density, suggesting their donor nature. Furthermore, the profiles reveal a clear trend: as the selenium content grows, the net charge density increases, leading to a narrower depletion region width. This observation is particularly significant given the thin nature of the layers since there is a risk of having a fully depleted absorber, which implies recombination at the back surface, limiting the voltage [26]. The sudden rise of the profiles towards the back contact for the thinner CdSe cases is a measurement artefact, indicating that the absorber is completely depleted [27], as also suggested by the arrows, which are located at a distance greater than 0.8 μm from the junction. 270 nm is an optimal CdSe thickness to achieve sufficient net charge density (approximately $2*10^5$ cm^{-3}) to reduce the depletion region width to around 500 nm; moreover, in this case, CV and DLCP profiles overlap, suggesting a reduced number of deep defects. In contrast, the sample fabricated using a 400 nm thick CdSe layer shows the highest concentration of deep defects, possibly due to the disordered arrangement of the grains and the voids seen with EBSD analysis.

4.2. Performance of the devices

But how does the impact of the selenium concentration on the absorber structure influence the performance of the devices? Table 1 presents the peak and average efficiency parameters of samples fabricated with different CdSe/CdTe ratios, while Fig. 10 shows the current-voltage characteristics of the best cells. By increasing the thickness of the CdSe layer from 75 to 270 nm, the average Voc slightly decreases, possibly due to the narrowing of the band gap at the junction; however, this leads to a mild rise of the Jsc. On the other hand, the FF has a more substantial improvement from 58 to 62 % on average. This could indicate reduced recombination in the depletion region [28] and thus be related to the increased selenium concentration since Se passivates grain boundaries and enhances carrier lifetime [19]. Overall, the efficiency of the cells increases modestly from 9.7 to 10 % on average. The slight difference in cell performance can also be observed by comparing the JVs of the peak cells in Fig. 10. By further increasing the thickness of CdSe to 400 nm, the performance of the devices drops to 5 % on average, due to the lowering of all the efficiency parameters; which is not surprising, given the previous analysis. The lower Jsc value, compared to the other samples, was already evident from the EQE measurements, which we related to the smaller size of the grains and their disordered arrangement due to the higher selenium concentration. However, the consequent enhanced carrier recombination also explains the Voc and FF drop.

Table 1
Peak and average efficiency parameters of samples fabricated with different CdSe/CdTe ratios.

Sample CdSe/CdTe		FF (%)	Voc (mV)	Jsc (mA/cm^2)	Eff (%)
75/725	Best	58	699	24.9	10.1
	Avg	58 ± 1	699 ± 1	23.8 ± 2	9.7 ± 0.6
150/650	Best	59	713	23.9	10.1
	Avg	58 ± 1	685 ± 37	24.1 ± 0.9	9.6 ± 0.4
270/530	Best	64	671	24.5	10.5
	Avg	62 ± 2	673 ± 4	24.3 ± 0.6	10.0 ± 0.4
400/400	Best	55	545	18.3	5.5
	Avg	52 ± 5	484 ± 82	20.0 ± 2	5.0 ± 0.7

Previous studies have demonstrated that Br-MeOH processes, being Cd-selective etchings, also convert regions of grain boundaries from CdTe to elemental Te, reducing their band gap to 0.33 eV. This can be seen as an extension of the back contact that diffuses into the bulk. Therefore, in the case of ultra-thin absorbers, the increased recombination due to elemental tellurium in the grain boundaries would lead to Voc losses [29].

For this reason, instead of using the Br-MeOH etching, recently, the back surface of the absorbers was washed with distilled water after the

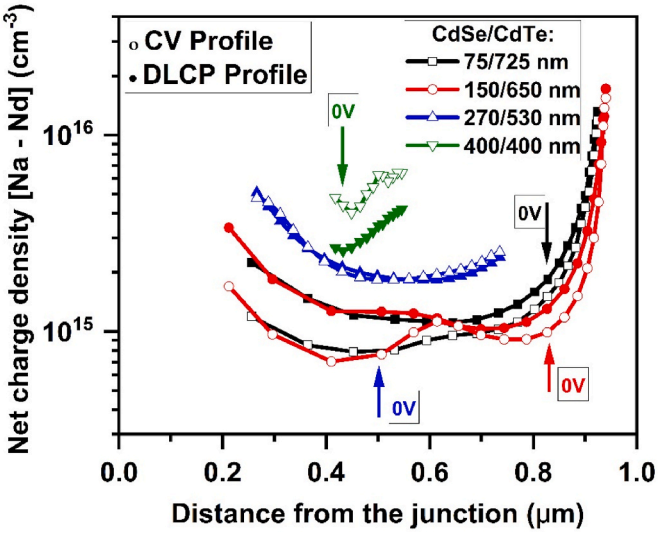

Fig. 9. Comparison between CV (open dots) and DLCP (full dots) profiles of samples fabricated with different CdSe/CdTe ratios.

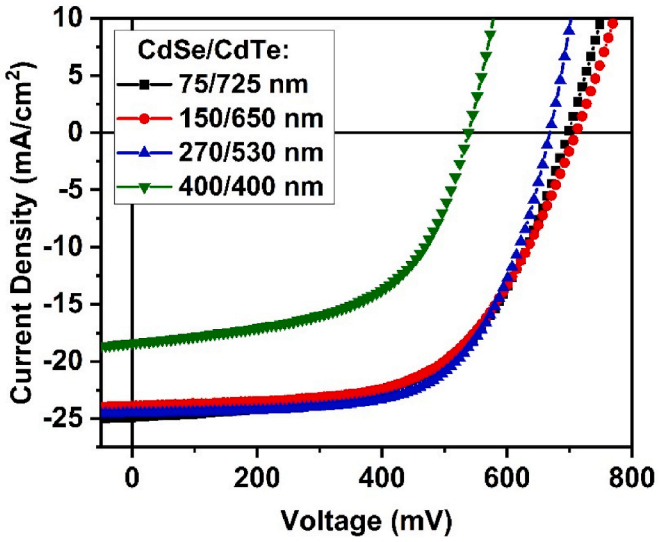

Fig. 10. JV-curves of the samples fabricated with different CdSe/CdTe ratios.

activation treatment. Avoiding the etching step allowed us to achieve higher-efficiency devices, whose JV curves are presented in Fig. 11 and the related efficiency parameters in Table 2. This optimization has strongly improved the average FF of all the samples and the Voc of the devices with the lowest Se concentration. Without elemental Te, the active layer is wider, reducing the risk of a fully depleted absorber. This is particularly effective for cells where the net charge density is reduced by low Se concentration.

Without the Br-methanol step, the 150/650 case is the best trade-off between the reduced band gap value at the junction and the increased net charge density, due to the insertion of selenium, reaching an average Voc of 753 mV. These cells have achieved peak efficiencies close to 13 %, which is noticeable considering the thin absorber (800 nm). Again, fabricating devices with a 1 to 1 CdSe/CdTe ratio results in a drop in all efficiency parameters.

4.3. Stability of the samples

The samples have been subjected to accelerated stability tests (AST), to investigate how the selenium concentration could affect the stability of the devices. Precisely, 10 cells for each type were kept at 80 °C under one sun illumination in an open circuit condition, and their efficiency parameters were periodically measured after cooling down; the average efficiency, FF, Jsc and Voc normalized to their initial values versus time are presented in Fig. 12. In this case, all the devices were subjected to the above-mentioned etching treatment. All samples show a stable current density over time, in line with what we have already reported for devices with a 7 μm thick CdTe absorber [30]; only the cells with the highest Se concentration show a slightly unstable Jsc. Except for the devices with an initial CdSe thickness of 75 nm, these thinner, selenium-containing samples demonstrate a more substantial Voc reduction than the thicker CdTe; in contrast, the FF is stable or even improved over time. Overall, samples with intermediate selenium concentrations show stability consistent with our CdS/CdTe devices; samples containing less selenium are more stable, while those fabricated with a CdSe/CdTe 1 to 1 ratio are more unstable. Thus, the degradation over time of the cells depends on the initial CdSe/CdTe ratio; by increasing Se concentration, the stability of the devices reduces. Se insertion strongly affects the degradation of the Voc. In CdS/CdTe cells, Voc degradation was attributed to Cu diffusion from the back contact; Cu is a fast diffuser that accumulates preferentially along grain boundaries, causing shunt paths and forming donor defects [30]. This AST proves that also Se causes instability, depending on its concentration. This does not appear to be

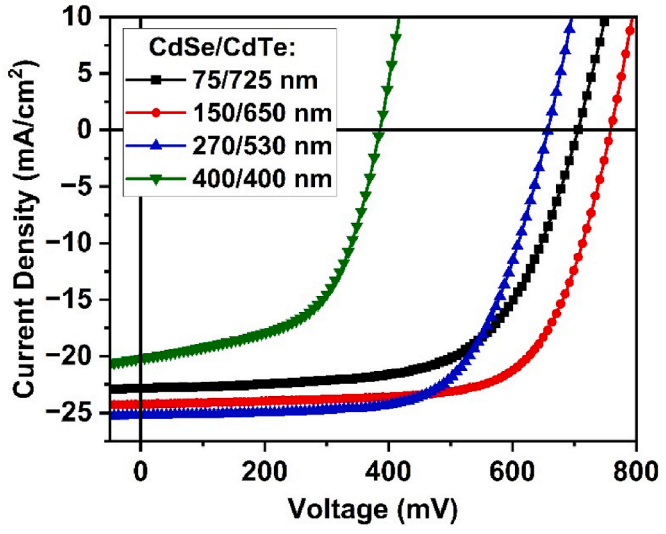

Fig. 11. JV curves of the samples fabricated with different CdSe/CdTe ratios without Br-MeOH etching.

Table 2
Peak and average efficiency parameters of samples fabricated with different CdSe/CdTe ratios without Br-MeOH etching.

Sample CdSe/CdTe		FF (%)	Voc (mV)	Jsc (mA/cm^2)	Eff (%)
75/725	Best	63	706	22.8	10.2
	Avg	61 ± 2	685 ± 25	23.1 ± 0.4	9.8 ± 0.5
150/650	Best	69	762	24.3	12.8
	Avg	67 ± 2	753 ± 11	24.6 ± 0.6	12.4 ± 0.4
270/530	Best	65	664	25.3	10.9
	Avg	64 ± 1	659 ± 4	25.4 ± 0.2	10.8 ± 0.2
400/400	Best	56	391	20.1	4.4
	Avg	56 ± 2	384 ± 7	20.1 ± 1	4.3 ± 0.1

due to an actual diffusion of selenium during the AST since the most unstable sample is 400/400, where the CdSeTe compound is already homogeneous throughout the thickness, and, therefore, the diffusion coefficient of Se should be minimal. One hypothesis could be that some defects formed by selenium are not stable and tend to change nature over time, as had already been seen for copper, where the decay of the acceptor Cu_{Cd} into the acceptor-donor pair Cu_i-V_{Cd} was observed [30]. On the other hand, this significant degradation of the devices could also be due to the copper itself since a higher concentration of selenium leads to the formation of smaller grains throughout the absorber, increasing the amount of grain boundaries and thus favouring the diffusion of Cu from the back contact towards the junction. Furthermore, in a thicker absorber, the reduction in the amount of copper at the back contact over time (due to its diffusion) leads to the roll-over effects, causing a decrease in FF. However, this effect is much less noticeable for thin absorbers where the space charge regions at the p–n junction and at the back contact tend to overlap [31].

5. Conclusions

CdSeTe/CdTe devices with reduced absorber thickness of 0.8 μm with different CdSe/CdTe ratios have been fabricated to study the impact of selenium concentration in ultra-thin absorbers. Thinning the absorber thickness has the advantage of reducing costs, material availability, and environmental effects; thus, it is now essential to understand the impact of selenium introduction in ultra-thin absorbers.

Interestingly, in these cells, there is no evidence of the CdSeTe/CdTe bi-layer structure observed in devices with thicker CdTe; here, selenium diffuses throughout the entire absorber, even using 75/725 nm of CdSe/CdTe. With this ratio, SIMS analysis suggests the formation of a graded band gap, with a decreasing concentration of Se towards the back contact; even if the hyperspectral CL map shows that the band gap of the absorber mainly changes from grain to grain, thus also parallel to the substrate. By increasing the CdSe/CdTe ratio, the measurements show a progressive reduction of the minimum band gap and an increase in the net charge density, thus demonstrating the insertion of Se into the lattice structure and its function of passivation of the grain boundaries. Furthermore, enhancing the net charge density narrows the depletion region width, a factor that should not be neglected given the thin absorber thickness; a completely depleted absorber leads to increased recombination in the back contact region.

On the other hand, by increasing the selenium concentration, a progressive decrease in grain size occurs along the entire thickness of the absorber. It is, therefore, not limited to the junction region alone. This inevitably increases the amount of grain boundaries and, hence, the possible carrier recombination. Using a CdSe/CdTe ratio of 1/1, a structure composed of small, disorderly-arranged grains is formed, with also the presence of voiding. This results in a marked reduction in quantum efficiency for all wavelengths and, consequently, a drop in device performance.

Selenium introduction also affects the stability of the devices: accelerated stability tests prove that by increasing Se concentration, the

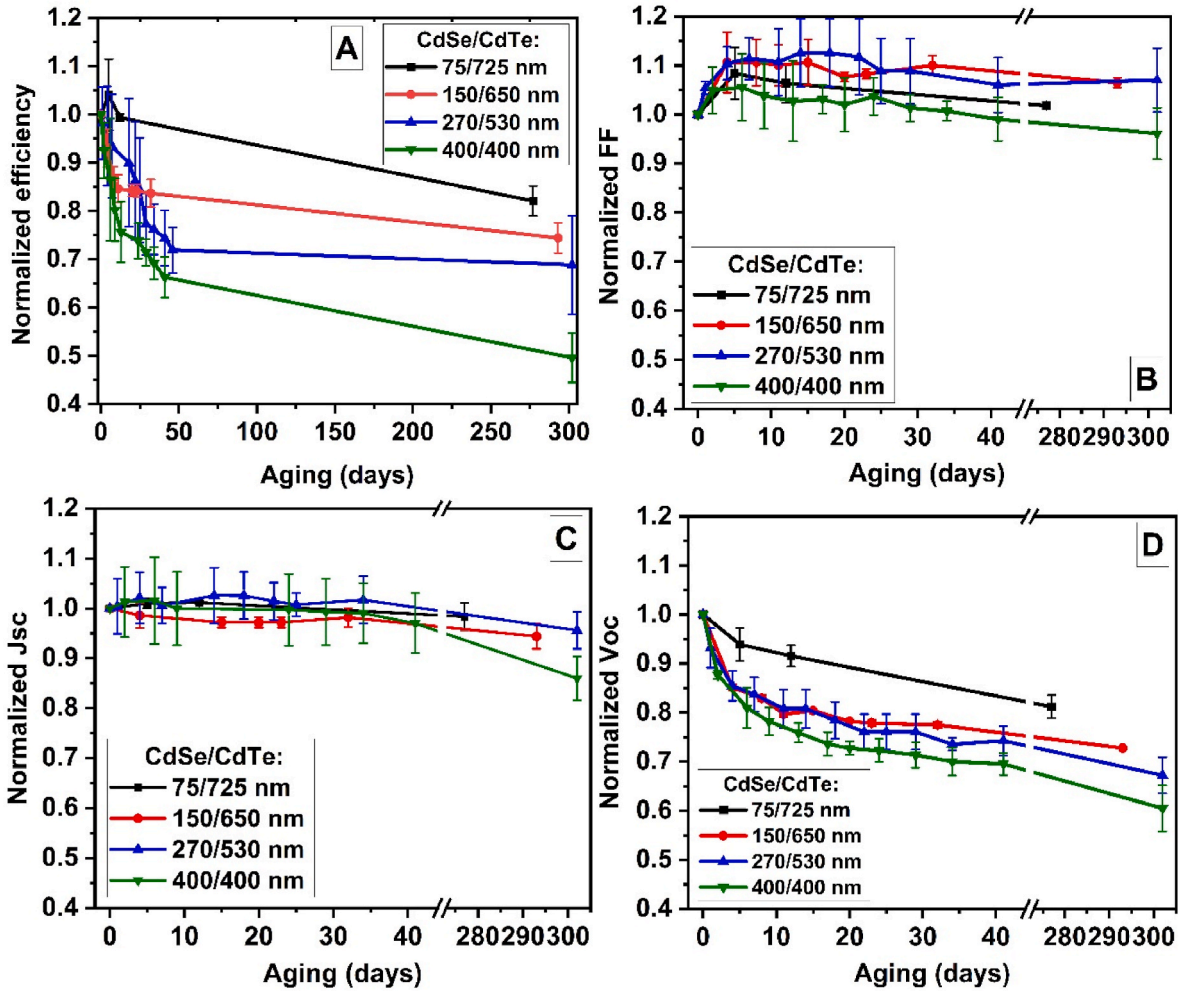

Fig. 12. Graphs reporting the performance degradation along time of the different CdSe/CdTe ratios samples. Normalized efficiency (A), FF (B), Jsc (C) and Voc (D) values at various time steps of AST.

stability of the cells reduces, mainly due to the degradation of Voc.

The 150/650 nm CdSe/CdTe samples fabricated without Br-MeOH etching demonstrate the best compromise between the effects of the selenium introduction mentioned above, leading to the highest performances. Currently, in our laboratory, these samples have reached a remarkable (considering the ultra-thin absorber) efficiency of 12.8 %.

The different Se concentrations in different grains have been attributed to the energetically favourable diffusion of Se through specific crystal orientations of CdTe compared to others. In a 2–3 μm thick as-deposited CdTe, a few layers of grains form the film thickness; thus, while diffusing through the grain boundaries, Se can surround the grains of the first layer/layers and enter through the preferred orientation into the matrix. On the other hand, if the grains extend throughout the entire thin thickness of the as-deposited CdTe, Se is disadvantaged during the activation treatment in accessing some grains, depending on their orientations. Moreover, starting from a CdTe film composed of a single layer of grains, it is impossible to obtain a CdSeTe/CdTe bi-layer; this limits the grain size growth throughout the absorber.

CRediT authorship contribution statement

Mariyam Mukhtar: Writing – original draft, Investigation. **Elisa Artegiani:** Writing – review & editing, Writing – original draft, Investigation, Data curation. **Sam Machin:** Investigation, Data curation. **Andrea Gasparotto:** Investigation. **Chiara Liliana Boldrini:** Investigation. **Giorgio Tseberlidis:** Investigation. **Simona Binetti:** Supervision. **Michael Walls:** Supervision. **Alessandro Romeo:** Writing – review & editing, Writing – original draft, Validation, Supervision, Methodology, Investigation, Funding acquisition, Data curation.

Declaration of competing interest

The authors declare that they have no known competing financial interests or personal relationships that could have appeared to influence the work reported in this paper.

Acknowledgements

The Technological Platform Center (CPT) at the University of Verona, in the person of Dr. Marco Giarola, is thankfully acknowledged for Raman measurements. The Loughborough authors are grateful to EPSRC through project EP/X030245/1 for funding the Cathodoluminescence facility.

Data availability

Data will be made available on request.

References

[1] M.A. Green, et al., Solar cell efficiency tables (version 66), Prog. Photovoltaics Res. Appl. (May 2025), https://doi.org/10.1002/pip.3919.

[2] M. Lingg, S. Buecheler, A.N. Tiwari, Review of CdTe1-xSex Thin Films in Solar Cell Applications, 2019, https://doi.org/10.3390/coatings9080520.
[3] M.A. Green, E.D. Dunlop, J. Hohl-Ebinger, M. Yoshita, N. Kopidakis, X. Hao, Solar cell efficiency tables (version 56), Prog. Photovoltaics Res. Appl. 28 (7) (2020) 629–638, https://doi.org/10.1002/pip.3303.
[4] T.A.M. Fiducia, et al., Understanding the role of selenium in defect passivation for highly efficient selenium-alloyed cadmium telluride solar cells, Nat. Energy 4 (6) (2019) 504–511, https://doi.org/10.1038/s41560-019-0389-z.
[5] M. Mukhtar, et al., Study of ultra-thin cadmium telluride solar cells, in: Conference Record of the IEEE Photovoltaic Specialists Conference, Institute of Electrical and Electronics Engineers Inc., 2024, pp. 648–651, https://doi.org/10.1109/PVSC57443.2024.10749595.
[6] X. Zhang, et al., High-performance ultra-thin CdTe solar cells with CuxByO back-buffer layer by a low-temperature solution processing, Sol. Energy Mater. Sol. Cell. 282 (Apr. 2025) 113447, https://doi.org/10.1016/J.SOLMAT.2025.113447.
[7] Y. Tai, et al., Research on ultra-thin cadmium telluride heterojunction thin film solar cells, Renew. Sustain. Energy Rev. 207 (Jan. 2025) 114996, https://doi.org/10.1016/J.RSER.2024.114996.
[8] A. Bosio, S. Pasini, N. Romeo, The history of photovoltaics with emphasis on CdTe solar cells and modules, Coatings 10 (4) (2020), https://doi.org/10.3390/coatings10040344.
[9] A. Salavei, I. Rimmaudo, F. Piccinelli, A. Romeo, Influence of CdTe thickness on structural and electrical properties of CdTe/CdS solar cells, Thin Solid Films 535 (1) (2013) 257–260, https://doi.org/10.1016/j.tsf.2012.11.121.
[10] M.A. Scarpulla, et al., Cdte-based Thin Film Photovoltaics: Recent Advances, Current Challenges and Future Prospects, 2023, https://doi.org/10.1016/j.solmat.2023.112289.
[11] V. Pecunia, et al., Roadmap on energy harvesting materials, JPhys Materials 6 (4) (2023), https://doi.org/10.1088/2515-7639/acc550.
[12] A. Romeo, E. Artegiani, D. Menossi, Low substrate temperature CdTe solar cells: a review, Sol. Energy 175 (Mar) (2018), https://doi.org/10.1016/j.solener.2018.02.038.
[13] E. Artegiani, A. Gasparotto, M. Meneghini, G. Meneghesso, A. Romeo, How the selenium distribution in CdTe affects the carrier properties of CdSeTe/CdTe solar cells, Sol. Energy 260 (2023), https://doi.org/10.1016/j.solener.2023.05.058.
[14] E. Artegiani, et al., A new method for CdSexTe1-x band grading for high efficiency thin-absorber CdTe solar cells, Sol. Energy Mater. Sol. Cell. 226 (Jul) (2021), https://doi.org/10.1016/j.solmat.2021.111081.
[15] I. Rimmaudo, et al., Improved stability of CdTe solar cells by absorber surface etching, Sol. Energy Mater. Sol. Cell. 162 (2017) 127–133, https://doi.org/10.1016/j.solmat.2016.12.044.
[16] D.E. Swanson, J.R. Sites, W.S. Sampath, Co-sublimation of CdSexTe1−x layers for CdTe solar cells, Sol. Energy Mater. Sol. Cell. 159 (2017) 389–394, https://doi.org/10.1016/j.solmat.2016.09.025.
[17] T. Ungár, Microstructural parameters from X-ray diffraction peak broadening, Scr. Mater. 51 (8) (2004) 777–781, https://doi.org/10.1016/j.scriptamat.2004.05.007.
[18] V. Kornienko, et al., Absorber texture and the efficiency of polycrystalline thin film CdTe solar cells, Thin Solid Films 793 (2024), https://doi.org/10.1016/j.tsf.2024.140277.
[19] X. Zheng, et al., Recombination and bandgap engineering in CdSeTe/CdTe solar cells, APL Mater. 7 (7) (2019), https://doi.org/10.1063/1.5098459.
[20] B.E. McCandless, S.S. Hegedus, R.W. Birkmire, D. Cunningham, Correlation of surface phases with electrical behavior in thin-film CdTe devices, Thin Solid Films (2003), https://doi.org/10.1016/S0040-6090(03)00266-9.
[21] N.R. Paudel, Y. Yan, Enhancing the photo-currents of CdTe thin-film solar cells in both short and long wavelength regions, Appl. Phys. Lett. 105 (18) (2014) 1–6, https://doi.org/10.1063/1.4901532.
[22] X. Liu, et al., The effect of remnant CdSe layers on the performance of CdSeTe/CdTe photovoltaic devices, Sol. Energy Mater. Sol. Cell. 267 (2024), https://doi.org/10.1016/j.solmat.2024.112717.
[23] J.M. Raguse, Electroluminescence of Thin-Film Cdte Solar Cells and Modules (Phd), Colorado State University, 2015 [Online]. Available: https://www.proquest.com/dissertations-theses/electroluminescence-thin-film-cdte-solar-cells/docview/1717099568/se-2.
[24] A. Shah, et al., Understanding the copassivation effect of Cl and Se for CdTe grain boundaries, ACS Appl. Mater. Interfaces 13 (29) (2021), https://doi.org/10.1021/acsami.1c06587.
[25] J.T. Heath, J.D. Cohen, W.N. Shafarman, Bulk and metastable defects in CuIn1-xGaxSe2 thin films using drive-level capacitance profiling, J. Appl. Phys. 95 (3) (2004) 1000–1010, https://doi.org/10.1063/1.1633982.
[26] J. Sites, J. Pan, Strategies to increase CdTe solar-cell voltage, Thin Solid Films (2007), https://doi.org/10.1016/j.tsf.2006.12.147.
[27] J.V. Li, et al., Theoretical analysis of effects of deep level, back contact, and absorber thickness on capacitance-voltage profiling of CdTe thin-film solar cells, Sol. Energy Mater. Sol. Cell. (2012), https://doi.org/10.1016/j.solmat.2012.01.003.
[28] S.H. Demtsu, J.R. Sites, Quantification of losses in thin-film CdS/CdTe solar cells, in: Conference Record of the thirty-first IEEE Photovoltaic Specialists Conference, IEEE, Jan. 2005, pp. 347–350, https://doi.org/10.1109/PVSC.2005.1488140.
[29] S. Misra, et al., Cadmium selective etching in CdTe solar cells produces detrimental narrow-gap Te in grain boundaries, ACS Appl. Energy Mater. 3 (2) (2020), https://doi.org/10.1021/acsaem.9b02224.
[30] E. Artegiani, J.D. Major, H. Shiel, V. Dhanak, C. Ferrari, A. Romeo, How the amount of copper influences the formation and stability of defects in CdTe solar cells, Sol. Energy Mater. Sol. Cell. 204 (Jan. 2020) 110228, https://doi.org/10.1016/j.solmat.2019.110228.
[31] M. Hädrich, C. Heisler, U. Reislöhner, C. Kraft, H. Metzner, Back contact formation in thin cadmium telluride solar cells, Thin Solid Films 519 (21) (2011) 7156–7159, https://doi.org/10.1016/j.tsf.2010.12.144.